Morphological Optimization for Tensegrity Quadruped Locomotion

Dawn Hustig-Schultz[1], Vytas SunSpiral[2,4], and Mircea Teodorescu[1]

***Abstract*— The increasing complexity of soft and hybrid-soft robots highlights the need for more efficient methods of minimizing machine learning solution spaces, and creative ways to ease the process of rapid prototyping. In this paper, we present an initial exploration of this process, using hand-chosen morphologies. Four different choices of muscle groups will be actuated on a tensegrity quadruped called MountainGoat: three for a primarily spine-driven morphology, and one for a primarily leg-driven morphology, and the locomotion speed will be compared. Each iteration of design seeks to reduce the total number of active muscles, and consequently reduce the dimensionality of the problem for machine learning, while still producing effective locomotion. The reduction in active muscles seeks to simplify future rapid prototyping of the robot.**

I. INTRODUCTION

As tensegrity structures and their control mechanisms become more complex, it is important to find strategies for keeping the dimensionality of the solution space small for more efficient performance and more successful machine learning outcomes. Iscen, et. al. have explored the use of coevolutionary algorithms to control underactuated tensegrities [1], to reduce solution space. Previous research into redundancy of actuators on the SUPERball tensegrity robot, by Lessard, et. al. has also shown that reduction in active muscles gracefully degrades productive locomotion, rather than curtailing it [2]. This study showed that the reduction of the dimensionality of the solution space for a tensegrity robot, which can help increase the chances of finding desirable solutions, will not necessarily harm the robot's performance and can ease the process of learning desirable locomotion solutions.

Due to the increasing complexity of tensegrity robots, rapid prototyping can be more challenging than for rigid-bodied robots. One major obstacle is the large amount of actuators that may be needed in order for a tensegrity quadruped to move effectively, even over flat terrain. Some promising potential solutions exist in the form of pneumatic actuators, as investigated by Polygerinos, et. al. [3] and Niiyama, et. al. [4], Shape Memory Alloys (SMAs) as implemented by Umedachi, et. al. [5], and dielectric elastomers, as explored by Pelrine, et. al. [6], Petralia et. al. [7], and Bilodeau, et. al. [8]. Many of these solutions, however, have drawbacks, such as heat dissipation and reliability for SMAs or the need for large volumes of air for pneumatics. Others, such as soft actuators, are still in early developmental stages. Initial rapid prototyping could potentially benefit from being able to use readily available, off-the-shelf parts, with reliance on more sophisticated actuators left to later prototypes. For more complex robotic morphologies, this means finding the most efficient approach to minimize the use of commercially available actuators.

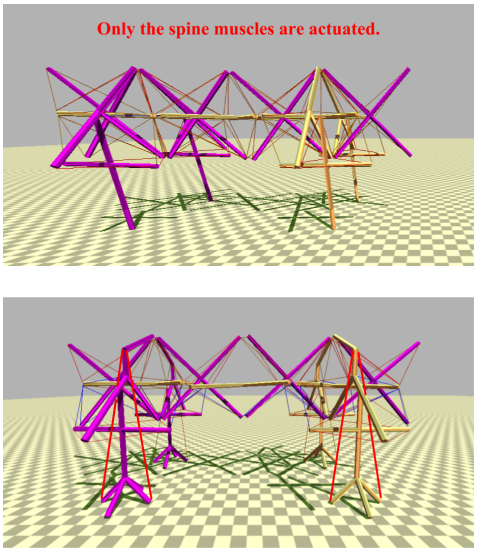

Fig. 1: Two different approaches to actuating *MountainGoat*. Top: This version of *MountainGoat* will be used for spine actuation only, implementing three different actuator configuations that use 52, 24, and 16 muscles. Bottom: This version of *MountainGoat*, called *Achilles*, will use leg actuation only. The muscles to be actuated are highlighted in red on only two of the legs in the figure, but will be actuated on all four legs.

For our exploration of solution space reduction, we will use two different quadruped morphologies. In our previous publication, we have discussed the centrality of the spine to locomotion [9], using the morphology seen in the top of Fig. 1. Besides the spine's central role in locomotion, a well-formed Achilles tendon also plays an important supporting role. Various research groups have found that, though the gastrocnemius muscle does little mechanical work, elastic energy storage and return from the Achilles tendon plays a major role in power production at the ankle of bipeds and quadrupeds [10], and that the absence of a well developed Achilles tendon would prevent bipeds from running effectively both at high speeds and over long distances [11]. This suggests the importance of having an Achilles tendon to help produce the necessary ground reaction force for

[1]University of California, Santa Cruz, Santa Cruz, CA 95064
[2]Authors with the NASA Ames Dynamic Tensegrity Robotics Lab, Moffett Field, CA 94035
[4]Stinger Ghaffarian Technologies, Greenbelt, MD 20770, USA

quadruped locomotion. Researchers at MIT have explored the advantages of an Achilles tendon in the Cheetah robot [12]. In the process of reducing our robot's solution space, we will also present preliminary findings of an an Achilles tendon, for which we will simulate the morphology shown in the bottom of Fig. 1. We will focus on a total of four different hand-chosen actuation solutions for the two morphologies mentioned above, one for the leg-driven morphology, and three for the spine-driven morphology.

II. BACKGROUND

Class-1 tensegrity structures consist of disjoint compression members interconnected by a system of tension members, with no two compression members in direct contact. Other class-k structures, with k equaling the number of compressive members that come into contact at a movable joint, also exist [13]. These structures were introduced in architecture by Kenneth Snelson [14], but more recently have been incorporated into robotics. As tensegrity structures typically have multiple tension members, which can be employed as actuators, they are robust to failure that can arise from the loss of one or more actuators [2]. Forces tend to distribute evenly across the web of tension members, which makes tensegrity structures impact tolerant and less likely to damage their surroundings.

The flexibility and impact tolerance of tensegrity structures make them ideal for locomotion over rugged terrain, as they are tolerant to perturbations, and prior studies with other tensegrity morphologies by Xydes, et. al. [15], Iscen, et. al. [16], and Mirletz, et. al. [17] have shown robust locomotion over rough terrain. Various morphologies can incorporate tensegrity. Xydes, et. al. have explored tensegrity duct climbing robots [15], Sabelhaus, et. al. have built rigid-legged quadrupeds with tensegrity spines [18], Mirletz, et. al. have researched tensegrity spine locomotion [17], Lessard, et. al. have developed tensegrity arms [19], and Agogino, et. al. are developing tensegrity for planetary rovers [20].

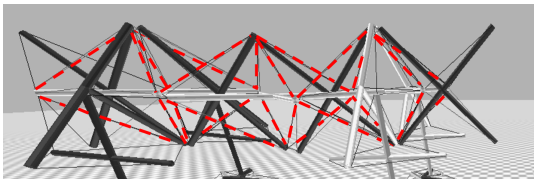

Fig. 2: An illustration of the muscle spirals, which consist of 24 active muscles, shown in red.

III. METHODS

A. Active Muscle Configurations

All our models are class-1 tensegrity structures, since compression members only connect via tension members. Our first active muscle configuration, *NoFeet*, consists of all 52 spine muscles as shown in Fig. 1.

Fig. 2 shows a configuration, *SpiralsOnly*, consisting of 24 active muscles shown in red. The passive cables, left unhighlighted, were left in the morphology as passive fascia in order to provide support to the structure. The choice to actuate only these muscles followed naturally from our previous work, in which these muscles gave extra torsion and support to the shoulders of *MountainGoat*. The question of interest here is whether actuating this set of spiral muscles alone will degrade performance, as previous studies have shown [2], while still allowing the morphology to still successfully carry out its intended function.

The third configuration, called *ReducedSpirals*, can be seen in Fig. 3, and consists of 16 active muscles in green. It is essentially the same as the active configuration of 24 muscles from Fig. 2, but with the first and last four muscles converted to passive fascia. Again, the question of interest is whether the reduction in the number of active muscles will gracefully degrade performance.

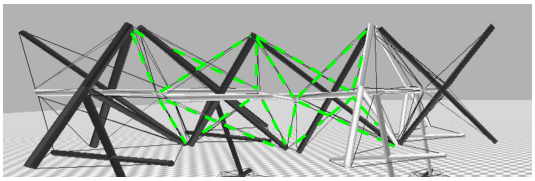

Fig. 3: An illustration of the shorter spirals, which consist of 16 active muscles, shown in green.

The bottom of Fig. 1 shows an active muscle configuration that depends on leg muscles, rather than spine muscles. This configuration, called *Achilles*, has an opposing pair of muscles in each leg, which act similarly to the combination of the gastrocnemius muscle and the Achilles tendon in many quadrupeds and bipeds. Since there are only two active leg muscles, the total number of active muscles for this configuration is 8. Additional rods in the feet of the model were added to increase stability during locomotion.

B. Control

The open source NASA Tensegrity Robotics Toolkit (NTRT), built on Bullet Physics Engine version 2.82, was used for simulation [1]. Internal cable and rigid body dynamics were previously validated within 1.3% error [21]. Additional tests validated steady state error on maximum cable tension within 6.1%, maximum system tension on hand-tuned controllers was validated within 7.9% error, and maximum cable tensions in simulations utilizing Central Pattern Generators (CPGs) were validated within 1.6% error [22].

Our approach to control continues upon our previous work [9] and that of Brian Mirletz, et. al. [17], which mimics the hierarchy of a biological nervous system [23]. This system utilizes impedance control for lower level reflexes [24], governed by the following equation:

$$T = T_0 + K(L - L_0) + B(V - V_0) \quad (1)$$

where T_0 is the tension offset and T is the output tension. K is the position gain on the difference between the current

[1]Source code for NTRT can be found at https://github.com/NASA-Tensegrity-Robotics-Toolkit

length L and the desired length L_0, and B is the velocity gain on the difference between the current velocity V and the desired trajectory V_0, where V_0 is the descending command from the CPG.

CPGs with feedback [25] [26], processed via a simple feedforward neural network, are used for higher level muscle group coordination. The equations for the CPGs are:

$$\dot{r}_i = \gamma(R_i + k_r F_r - r_i^2) r_i \tag{2.1}$$

$$\dot{\theta}_i = \omega_i + k_\theta F_\theta + \sum_j r_j w_{ij} sin(\theta_j - \theta_i - \phi_{ij}) \tag{2.2}$$

$$\dot{\omega}_i = k_\omega F_\omega \sin(\theta_i) \tag{2.3}$$

$$\dot{V}_i = r_i \cos(\theta_i) \tag{2.4}$$

The parameters r_i, ω_i, and θ_i are the CPG wave's amplitude, frequency, and phase, respectively. The convergence parameter γ and setpoint R_i are used to set the amplitude r_i. The coupling weight w_{ij}, phase offset ϕ_{ij}, and the the amplitude of the neighboring node r_j are used to determine the derivative of the phase $\dot{\theta}_i$. The feedback inputs F_r, F_θ, and F_ω have corresponding constant scalar gains k_r, k_θ, and k_ω. The resulting V_i from equation 2.4 is used as input to the lower level impedance controller.

C. Machine Learning

Our machine learning approach is based off our previous work [9] and that of Mirletz, et. al. [27], where learning runs consist of Monte Carlo (MC) trials followed by a genetic evolution stage. For all three spine muscle configurations, 30,000 random MC trials were performed. In these trials, neural network weights, CPG coupling weights, and CPG phase offsets are randomly generated. For the active muscle configuration consisting of leg muscles, 90,000 MC trials were performed, to accommodate for the extra PD and impedance controller parameters that generated in addition to the initial neural network weights, coupling weights, and phase offsets. All MC trials were 60 seconds in length.

For the evolution stage, the population consists of the best 40 results from MC, and evolution terminates after 60 generations. Each generation of evolution employs crossover, mutation, and elitism. During each generation, 15 of the 40 population members mutate, with each parameter in one member having a 50% chance of changing by a deviation of 0.03. Crossover is achieved by combining different groups of parameters from different population members. Crossover results in 10 new population members in the next generation, which by elitism replace the worst 10 from the current generation.

Our primary fitness function is distance, but the cost of transport (COT) is also considered. The distance is measured as follows: the x and z coordinates of the robot's center of mass (COM) are recorded at the beginning of a 60-second simulation, and then these coordinates are recorded again at the end of a simulation. The distance formula is then calculated using these two points. The cost of transport [28] is calculated as follows:

$$COT = \frac{W}{mgd} \tag{3}$$

W denotes work put into the system, while m, g, and d are the mass, gravity, and distance traveled, respectively. COT is a unitless metric, and a smaller COT means the system is more efficient. As can be seen from equation 3, gravity is also considered in simulation, and reflects Earth's gravity of $9.81 \frac{m}{s^2}$.

Our active leg configuration, *Achilles*, which employs antagonistic pairs of long muscles, required re-tuning of the PD and impedance controller parameters, which previously were tuned for shorter muscles. While these parameters can be tuned by hand, requiring time, trial, and error, our approach to tuning these parameters uses machine learning. Mirletz, et. al. experimented previously with machine-learned Impedance control parameters for tension, length, and velocity [29]. In addition to this, the proportion and derivative input parameters for PD control are learned via evolution.

For the configuration consisting of only leg muscles, we used a similar approach for reducing the solution space as in [28]. That is, our solution space consists of the coupling weights and phase offsets of one leg, and those parameters were reused for all four legs. This approach could be modified to produce different gaits by adding an offset pair for each leg to the individual weight-coupling pairs. The result would be the generation of different gaits, while still keeping the solution space small. Currently, our preliminary research does not yet utilize such a gait-dependent offset pair, but future work will explore different gaits using this technique.

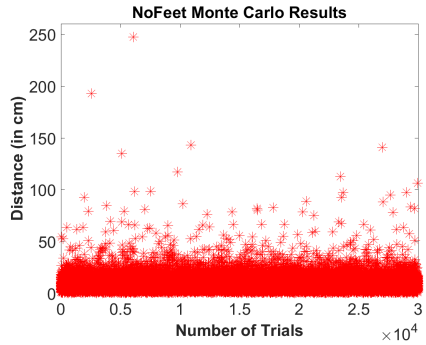

Fig. 4: The initial 30,000 randomized MC trials, each one minute in duration, for *NoFeet*. For the evolutionary results of the best 40 of these trials, see table I.

IV. RESULTS AND DISCUSSION

A. Control

The results of 30,000 MC trials on *NoFeet*, illustrated in the top of Fig. 1 above, can be seen in Fig. 4. This configuration yielded a distance of 247.1 cm/min after MC, longer than both *SpiralsOnly* and *ReducedSpirals*, with 24 actuators and 16 actuators, respectively. *NoFeet* produced many more

trials which traveled further than the 50 cm/minute threshold than either *SpiralsOnly* or *ReducedSpirals* did. The distance after evolution, which was 339.4 cm/min, is listed in table I.

The MC results for *SpiralsOnly*, depicted in Fig. 2, can be seen in Fig. 5. The number of trials faster than 50 cm/min is much sparser than for *NoFeet*, which is consistent with the results in Lessard, et. al. [2]. However, the best trial traveled at a speed of 229.4 cm/min, which though slower than the best trial for *NoFeet*, as seen in in figure 4, is nonetheless close. Despite the sparsity of trials faster than 50 cm/min, *SpiralsOnly* improved the most during evolution. This evolution result could be due to the fact that *SpiralsOnly* had at least one more trial with a distance longer than 150 cm/minute than *NoFeet* had. The favorable traits from this extra MC trial would most likely give it an advantage over multiple generations. As seen in table I and figure 8, the distance traveled increased to 365.8 cm/min after evolution.

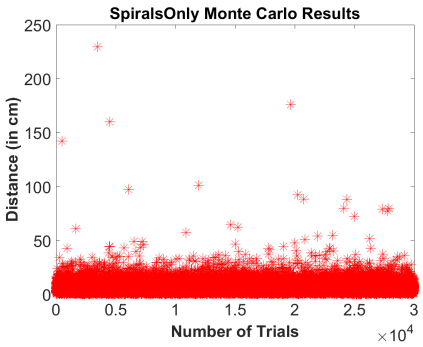

Fig. 5: The initial 30,000 randomized MC trials, each one minute in duration, for *SpiralsOnly*. See table I and Fig. 8 for the resulting distance after evolution from the best 40 of these trials.

Fig. 6 shows the results of 30,000 MC trials for *ReducedSpirals* in Fig. 3. As with *SpiralsOnly*, there is a sparser number of trials faster than the 50 cm/min threshold *ReducedSpirals* than there is for *NoFeet*. The use of 16 spine actuators resulted in a best trial of 150.2 cm/minute, which was slower than the best trials for both *SpiralsOnly* and *NoFeet*. The results of evolution increased the speed to 274.7 cm/min as in table I and figure 8. In our previous work, we discussed the importance of this type of spiral cable configuration for increasing torsion in the spine and giving more shoulder support for lifting the legs [9]. The resulting performance of *ReducedSpirals*, in comparison to *SpiralsOnly*, supports this claim, inasmuch as decreasing the length of this spiral leads to decreased torsion and shoulder support. Also, the general reduction in the number of actuators supports graceful degradation, rather than sharp cessation, in performance.

Since we use machine learning to tune the PD and impedance parameters for *Achilles*, we ran three times the amount of MC trials. Fig. 7 shows the results of these 90,000 trials. The best trial for *Achilles*, at 458.3 cm/min, is roughly three times as fast as *NoFeet*, *SpiralsOnly*, and *ReducedSpirals* after MC, and is even faster than the evolved results for these other three cable configurations, at 779.3 cm/min. Figure 7 shows that the majority of the trials are concentrated below a threshold of 200 cm/min, which is much higher than the 50 cm/min threshold of *SpiralsOnly*, *ReducedSpirals*, and , *NoFeet*. Also, the results in the upper half of this plot are not quite as sparse as they are for the other experiments. This indicates that running more MC trials would improve our evolutionary results. It is quite possible that the strong ground reaction forces generated with the help of these long, antagonistic pairs, contributes to this increase in speed. Considering the centrality of the spine for locomotion, as hypothesized by Gracovetsky, et. al. [30], as well as the importance of the Achilles tendon for push off, as extensively explored by Folkertsma, et. al. [31], it would be interesting to see how combining both these types of active muscles would affect locomotion speed.

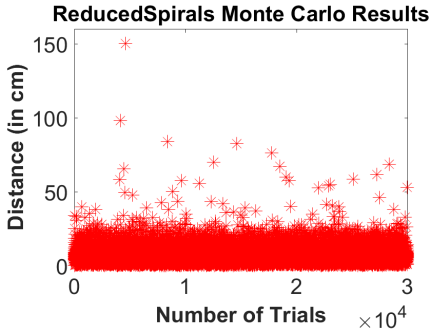

Fig. 6: The initial 30,000 randomized MC trials, each one minute in duration, for *ReducedSpirals*. See table I and Fig. 8 for the resulting distance after evolution from the best 40 of these trials.

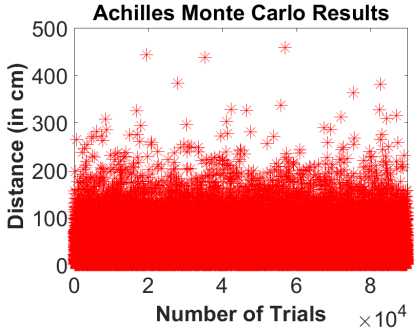

Fig. 7: The initial 90,000 randomized MC trials, each one minute in duration, for *Achilles*. For the results of the best 40 of these trials, see table I and Fig. 8.

Fig. 8 shows the progress of evolution for *NoFeet*, *SpiralsOnly*, *ReducedSpirals*, and *Achilles*. The most improvement occurs within the first 20 generations of evolution, leaving relatively minor improvements to the last 40 generations. This shows that our genetic algorithm converges quickly to the most advantageous solutions for a given morphology. *ReducedSpirals* both begins and ends the evolutionary stage as the slowest of all four actuator configurations, although

during generations three through eleven it is tied with *SpiralsOnly*. Although *SpiralsOnly* and *NoFeet* start out close in performance, *NoFeet* overtakes *SpiralsOnly* as early as the tenth generation. Nevertheless, *SpiralsOnly* barely wins out over *NoFeet* by generation 30. *Achilles* starts out performing better than *SpiralsOnly* and *ReducedSpirals*, and continues to outperform both throughout the entire evolution stage.

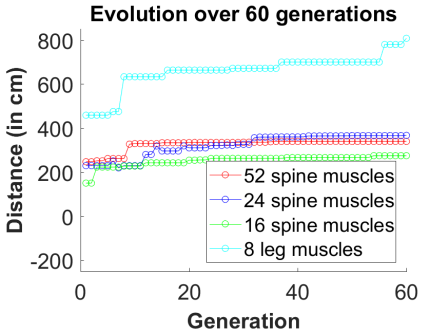

Fig. 8: A comparison of the progression of genetic evolution for *NoFeet* (red), *SpiralsOnly* (blue), *ReducedSpirals* (green), and *Achilles* (cyan).

TABLE I: Longest Distance Per Minute for Each Model

Model	Monte Carlo	Evolution
NoFeet	247.1 cm/min	339.4 cm/min
SpiralsOnly	229.4 cm/min	365.8 cm/min
ReducedSpirals	150.2 cm/min	274.7 cm/min
Achilles	458.3 cm/min	779.3 cm/min

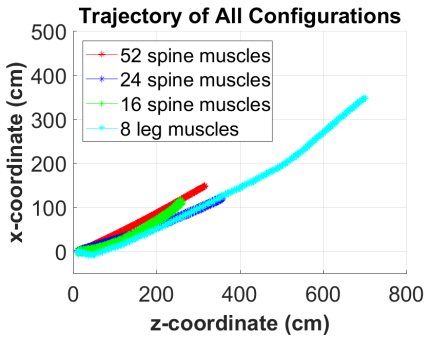

Fig. 9: The trajectories of all active muscle configurations, based on the center of mass of each robot. *NoFeet* is in red, *SpiralsOnly* is in blue, *ReducedSpirals* is in green, and *Achilles* is in cyan.

Fig. 9 compares the resulting trajectories of the various active muscle configurations. The paths traveled are the results after evolution, and the distances are listed in table I. When plotted, some of the trajectories were rotated with respect to the origin in order to better compare distance. Note that all trajectories are, for the most part, straight. The distances, however, are very different. These different distances support the concept, which we discussed in our previous work [9], that morphological design and control are highly coupled. A relatively minor reduction in the number of active cables from 24 to 16, for instance, caused a notable decrease in the speed of locomotion. A change in mode of actuation, from spine-driven to leg-driven locomotion, resulted in a notable increase in the speed of locomotion.

TABLE II: Cost of Transport for Each Model

Model	Monte Carlo	Evolution
NoFeet	3.18	1.68
SpiralsOnly	2.05	1.23
ReducedSpirals	1.80	1.09
Achilles	1.19	0.65

Table II shows the COT for each configuration, both for the best MC distance and for the best distance after evolution. Note that COT decreases as the number of active muscles decreases. This makes sense as reducing the number of actuators will also reduce the amount of energy necessary for locomotion. Also note that COT for each configuration is almost halved after evolution. This shows that our evolutionary algorithm not only increases the distance traveled, but also increases the efficiency in traveling this longer distance.

B. Solution Space

TABLE III: Number of parameter pairs learned for each model

Model	Active Muscles	Max per Segment	coupling pairs
NoFeet	52	16	392
SpiralsOnly	24	8	100
ReducedSpirals	16	8	100
Achilles	8	2	7

Mirletz et. al., in their earlier analysis of solution space dimensionality of CPG networks, arrived at the following formula for the number of possible coupling weight and phase offset pairs that a morphology with repeating segments and bi-directional CPG couplings would be required to learn for productive motion [28]:

$$CPG\ couplings = \frac{m(3m+1)}{2} \tag{3}$$

with m representing the number of active muscles, and hence number of active CPG nodes, per segment. *NoFeet*, shown in Fig. 1, has 16 nodes per segment, while *SpiralsOnly* and *ReducedSpirals* each have 8 nodes per segment. *Achilles* has only 2 nodes per leg. As seen in table III, this equates to a larger solution space for *NoFeet*, which requires learning 392 coupling pairs. The other spine configurations, *SpiralsOnly* and *ReducedSpirals*, have smaller solution spaces, with 100 coupling pairs. In contrast, *Achilles* has only 7 coupling pairs to be learned. Despite the fact that *Achilles* has extra PD and impedance controllers parameters to learn, these only account for 5 more variables, and thus this configuration has the smallest solution space of all four configurations.

V. CONCLUSIONS AND FUTURE WORK

We explored several active muscle configurations for *MountainGoat*, with each configuration reducing the solution space and improving speed and COT over the original. *SpiralsOnly* resulted in a longer distance than *NoFeet*, while *ReducedSpirals* was slower. Both *SpiralsOnly* and *ReducedSpirals* had lower COT than *NoFeet*, however. *Achilles* showed the most improvement in speed and COT of all the configurations. Future work will include verification of these results with construction of actuated prototypes, to test the practicality of the various designs.

As the long term goal for *MountainGoat* is robust terrain traversal, future work will also include integrating spine and leg muscle activation presented here, both in simulation and in prototype, with the goal of giving more support for lifting legs over obstacles. Different gaits will also be explored, using gait-dependent offset pairs for individual legs.

ACKNOWLEDGMENT

The authors would like to thank members of the NASA Ames Intelligent Robotics Group as well as the Advanced Studies Laboratories (ASL) for their support.

REFERENCES

[1] A. Iscen, K. Caluwaerts, J. Bruce, A. Agogino, V. SunSpiral, and K. Tumer, "Learning tensegrity locomotion using open-loop control signals and coevolutionary algorithms," *Artificial life*, 2015.

[2] S. Lessard, J. Bruce, A. Agogino, V. SunSpiral, and M. Teodorescu, "Robust Monte Carlo Control Policies to Maneuver Tensegrity Robots out of Obstacles," in *Proceedings of Autonomous Robots and Multi-robot Systems (ARMS), May 2015, Istanbul, Turkey*, 2015.

[3] P. Polygerinos, S. Lyne, Z. Wang, L. F. Nicolini, B. Mosadegh, G. M. Whitesides, and C. J. Walsh, "Towards a soft pneumatic glove for hand rehabilitation," in *2013 IEEE/RSJ International Conference on Intelligent Robots and Systems*. IEEE, 2013, pp. 1512–1517.

[4] R. Niiyama, C. Rognon, and Y. Kuniyoshi, "Printable pneumatic artificial muscles for anatomy-based humanoid robots," in *Humanoid Robots (Humanoids), 2015 IEEE-RAS 15th International Conference on*. IEEE, 2015, pp. 401–406.

[5] T. Umedachi, V. Vikas, and B. Trimmer, "Softworms: the design and control of non-pneumatic, 3d-printed, deformable robots," *Bioinspiration & biomimetics*, vol. 11, no. 2, p. 025001, 2016.

[6] R. Pelrine, R. D. Kornbluh, Q. Pei, S. Stanford, S. Oh, J. Eckerle, R. J. Full, M. A. Rosenthal, and K. Meijer, "Dielectric elastomer artificial muscle actuators: toward biomimetic motion," in *SPIE's 9th Annual International Symposium on Smart Structures and Materials*. International Society for Optics and Photonics, 2002, pp. 126–137.

[7] M. T. Petralia and R. J. Wood, "Fabrication and analysis of dielectric-elastomer minimum-energy structures for highly-deformable soft robotic systems," in *Intelligent Robots and Systems (IROS), 2010 IEEE/RSJ International Conference on*. IEEE, 2010, pp. 2357–2363.

[8] R. A. Bilodeau, E. L. White, and R. K. Kramer, "Monolithic fabrication of sensors and actuators in a soft robotic gripper," in *Intelligent Robots and Systems (IROS), 2015 IEEE/RSJ International Conference on*. IEEE, 2015, pp. 2324–2329.

[9] D. Hustig-Schultz, V. SunSpiral, and M. Teodorescu, "Morphological Design for Controlled Tensegrity Quadruped Locomotion," in *Proceedings of 2016 IEEE/RSJ International Conference on Intelligent Robots and Systems (IROS)*. IEEE, Oct. 2016, pp. 4714–4719.

[10] D. P. Ferris, G. S. Sawicki, and M. A. Daley, "A physiologist's perspective on robotic exoskeletons for human locomotion," *International Journal of Humanoid Robotics*, vol. 4, no. 03, pp. 507–528, 2007.

[11] G. Singh, V. P. Agrawal, M. Basavarajappa, and M. Manohar, "Gastrocnemius-achilles tendon-axis: A human anatomical variation," *International Journal of Biomedical and Advance Research*, vol. 3, no. 8, pp. 653–655, 2012.

[12] A. Ananthanarayanan, M. Azadi, and S. Kim, "Towards a bio-inspired leg design for high-speed running," *Bioinspiration & biomimetics*, vol. 7, no. 4, p. 046005, 2012.

[13] R. E. Skelton, R. Adhikari, J.-P. Pinaud, W. Chan, and J. Helton, "An introduction to the mechanics of tensegrity structures," in *Decision and Control, 2001. Proceedings of the 40th IEEE Conference on*, vol. 5. IEEE, 2001, pp. 4254–4259.

[14] K. Snelson, "Continuous tension, discontinuous compression structures. united states patent 3169611," Feburary 1965.

[15] A. L. Xydes, "Simulating ductt and optimizing control for ductt with machine learning," Ph.D. dissertation, University of California, San Diego, 2015.

[16] A. Iscen, A. Agogino, V. SunSpiral, and K. Tumer, "Robust distributed control of rolling tensegrity robot," in *The Autonomous Robots and Multirobot Systems (ARMS) workshop at AAMAS 2013*, 2013.

[17] B. T. Mirletz, P. Bhandal, R. D. Adams, A. K. Agogino, R. D. Quinn, and V. SunSpiral, "Goal-Directed CPG-Based Control for Tensegrity Spines with Many Degrees of Freedom Traversing Irregular Terrain," *Soft Robotics*, vol. 2, no. 4, pp. 165–176, 2015.

[18] A. P. Sabelhaus, H. Ji, P. Hylton, Y. Madaan, C. Yang, A. M. Agogino, J. Friesen, and V. SunSpiral, "Mechanism design and simulation of the ultra spine: A tensegrity robot," in *ASME 2015 International Design Engineering Technical Conferences and Computers and Information in Engineering Conference*. American Society of Mechanical Engineers, 2015, pp. V05AT08A059–V05AT08A059.

[19] S. Lessard, D. Castro, W. Asper, S. Chopra, L. Baltaxe-Admony, M. Teodorescu, V. SunSpiral, and A. Agogino, "A bio-inspired tensegrity manipulator with multi-dof, structurally compliant joints," to appear in Proceedings of the 2016 IEEE/RSJ International Conference on Intelligent Robots and Systems (IROS). IEEE, 2016.

[20] A. Agogino, V. SunSpiral, and D. Atkinson, "Super Ball Bot - structures for planetary landing and exploration," *NASA Innovative Advanced Concepts (NIAC) Program, Final Report*, 2013.

[21] K. Caluwaerts, J. Despraz, A. Işçen, A. P. Sabelhaus, J. Bruce, B. Schrauwen, and V. SunSpiral, "Design and control of compliant tensegrity robots through simulation and hardware validation," *Journal of The Royal Society Interface*, vol. 11, no. 98, p. 20140520, 2014.

[22] B. T. Mirletz, I.-W. Park, R. D. Quinn, and V. SunSpiral, "Towards bridging the reality gap between tensegrity simulation and robotic hardware," in *Intelligent Robots and Systems (IROS), 2015 IEEE/RSJ International Conference on*. IEEE, 2015, pp. 5357–5363.

[23] S. Grillner, A. Kozlov, P. Dario, C. Stefanini, A. Menciassi, A. Lansner, and J. H. Kotaleski, "Modeling a vertebrate motor system: pattern generation, steering and control of body orientation," *Progress in brain research*, vol. 165, pp. 221–234, 2007.

[24] O. Orki, A. Ayali, O. Shai, and U. Ben-Hanan, "Modeling of caterpillar crawl using novel tensegrity structures," *Bioinspiration & biomimetics*, vol. 7, no. 4, p. 046006, 2012.

[25] L. Righetti, J. Buchli, and A. J. Ijspeert, "Dynamic hebbian learning in adaptive frequency oscillators," *Physica D: Nonlinear Phenomena*, vol. 216, no. 2, pp. 269–281, 2006.

[26] S. Gay, J. Santos-Victor, and A. Ijspeert, "Learning robot gait stability using neural networks as sensory feedback function for central pattern generators," in *Intelligent Robots and Systems (IROS), 2013 IEEE/RSJ International Conference on*. IEEE, 2013, pp. 194–201.

[27] B. T. Mirletz, R. D. Quinn, and V. SunSpiral, "CPGs for Adaptive Control of Spine-like Tensegrity Structures," in *Proceedings of 2015 International Conference on Robotics and Automation (ICRA2015) Workshop on Central Pattern Generators for Locomotion Control: Pros, Cons & Alternatives*, 2015.

[28] B. Mirletz, I.-W. Park, T. E. Flemons, A. K. Agogino, R. D. Quinn, and V. SunSpiral, "Design and control of modular spine-like tensegrity structures," in *The 6th World Conference of the International Association for Structural Control and Monitoring (6WCSCM)*, 2014.

[29] B. T. Mirletz, "Adaptive central pattern generators for control of tensegrity spines with many degrees of freedom," Ph.D. dissertation, Case Western Reserve University, 2016.

[30] S. Gracovetsky, "An hypothesis for the role of the spine in human locomotion: a challenge to current thinking," *Journal of biomedical engineering*, vol. 7, no. 3, pp. 205–216, 1985.

[31] G. A. Folkertsma, S. Kim, and S. Stramigioli, "Parallel stiffness in a bounding quadruped with flexible spine," in *2012 IEEE/RSJ International Conference on Intelligent Robots and Systems*. IEEE, 2012, pp. 2210–2215.